

Multicellular Self-Organization of *P. aeruginosa* due to Interactions with Secreted Trails

Anatolij Gelimson,¹ Kun Zhao,^{2,3} Calvin K. Lee,³ W. Till Kranz,¹ Gerard C. L. Wong,^{3,*} and Ramin Golestanian^{1,†}

¹Rudolf Peierls Centre for Theoretical Physics, University of Oxford, Oxford OX1 3NP, United Kingdom

²Key Laboratory of Systems Bioengineering, Ministry of Education, School of Chemical Engineering and Technology, Tianjin University, Tianjin, 300072, People's Republic of China

³Bioengineering Department, Chemistry and Biochemistry Department, California Nano Systems Institute, UCLA, Los Angeles, California 90095-1600, USA

(Received 12 May 2016; published 20 October 2016)

Guided movement in response to slowly diffusing polymeric trails provides a unique mechanism for self-organization of some microorganisms. To elucidate how this signaling route leads to microcolony formation, we experimentally probe the trajectory and orientation of *Pseudomonas aeruginosa* that propel themselves on a surface using type IV pili motility appendages, which preferentially attach to deposited exopolysaccharides. We construct a stochastic model by analyzing single-bacterium trajectories and show that the resulting theoretical prediction for the many-body behavior of the bacteria is in quantitative agreement with our experimental characterization of how cells explore the surface via a power-law strategy.

DOI: 10.1103/PhysRevLett.117.178102

Chemotaxis—biasing motility in response to chemicals—is a fundamental organizing principle for guided movement in biological systems. Because of the long-range nature of the effect, it can strongly impact the dynamic organization of living [1–8] and synthetic [9–12] active matter. Chemotactic phenomena, with their implicit interpenetration between signal processing and migratory strategy [13,14], have a diverse range, although they are often studied in the limit when the chemicals diffuse much faster than the cells. It is interesting to examine the opposite extreme and investigate a highly competitive, noisy system where every cell-secreted signal is long lived and effectively nondiffusive. A model system for this scenario is *Pseudomonas aeruginosa*, which can secrete exopolysaccharides (EPS) [15–17]. *P. aeruginosa* moves on a 2D surface using the twitching motility mode via an EPS-binding motility appendage [Fig. 1(a)] known as a type IV pilus [18–23]. Recent work has shown that EPS play a key role in the clustering of cells into a microcolony [24], the first social step in bacterial biofilm formation, by facilitating pilus attachment. However, a quantitative understanding of the transition from single-bacterium motion to collective patterns is needed.

In the *P. aeruginosa* system, the EPS surface distribution that impacts a cell trajectory is dependent on the history of all other secreting cells that have traversed the surface, due to the long-lived nature of the Psl signal on the surface. This serves as a communal memory of particle trajectories and leads to a coupling between cells that have large spatio-temporal separations. This provides the dominant mechanism for self-organization in the dilute regime, which is relevant for early stages of biofilm formation; in the dense regime, other effects such as excluded volume interaction

[25], alignment [26–30], depletion interaction [31], etc., will also impact the collective behavior of the system [32].

Here, we present a quantitative description of how the microscopic motion of a single EPS-depositing bacterium directly leads to clustering and microcolony formation in the collective case. We (1) experimentally probe single-bacterium dynamics by measuring the trajectories and bacterial orientations (see Fig. 1), (2) theoretically derive a microscopic model for pili-driven motility, (3) extract all parameters on a single-particle level from experiments, and (4) show that the same model quantitatively explains experimentally measured observables in the early stages of biofilm formation, without any additional adjustments (see Figs. 2 and 3). Our multiscale description provides a quantitative understanding of how cells interact with their system of mutually secreted trails and spontaneously explore the surface via a power-law migratory strategy. A crucial consequence of type IV pilus sensing is the emergence of novel features in the orientational dynamics [33], which we fully characterize both experimentally and theoretically.

In our experiments, we used the *P. aeruginosa* PAO1 [34] strain $\Delta P_{psl}/P_{BAD-psl}$ [15], which is a strain with inducible Psl secretion controlled by arabinose concentrations. For the detailed experimental information, see the methods in Ref. [24]. An overnight bacteria culture in a FAB medium [35] supplemented with 30 mM glutamate was diluted and injected into a flow cell [24,36]. The FAB medium with 0.6 mM glutamate was continuously pumped through the flow chamber using a syringe pump with a flow rate of 3 mL/h at 30 °C. Different amounts of arabinose were added into the medium to control the production of Psl. Bright-field images were taken every three seconds by an electron multiplying charge coupled device camera on an Olympus

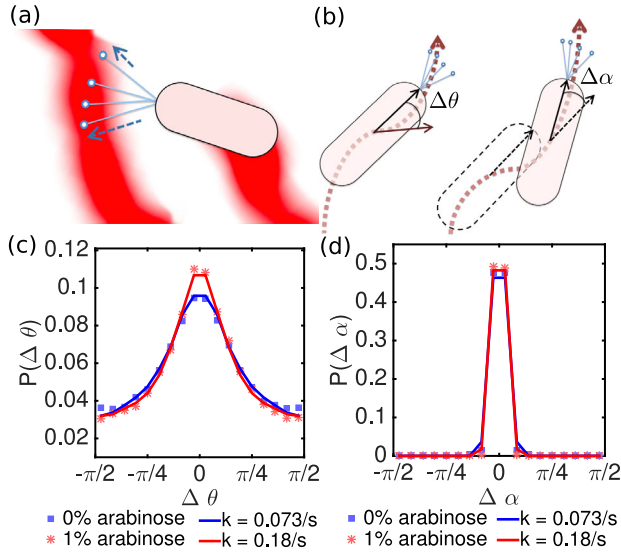


FIG. 1. (a) Bacterial model. Pili (light blue lines and circles) preferentially attach to secreted Psl films on the surface (red areas) and pull the bacterium forward. (b) Schematic illustration for the angles $\Delta\theta$ (left) and $\Delta\alpha$ (right). $\Delta\theta$ is the angle between the current body orientation and the bacterial trajectory (dotted lines), smoothed over 21 points, which have been recorded every 3 s, using a Savitzky-Golay filter of third order. $\Delta\alpha$ is the change in orientation between two time steps of 3 s. The resolution of an angle measurement is $\pm 5^\circ$, and about 400 000 angle measurements were performed at an early stage in a sparse population. (c) The best fits between the experimental (dots) and simulated (solid lines) distributions for $\Delta\theta$ (for different arabinose concentrations corresponding to different EPS secretion rates k). (d) The corresponding $\Delta\alpha$ distributions.

IX81 microscope equipped with a zero drift autofocus system. The image size is $67 \times 67 \mu\text{m}^2$ ($1024 \times 1024 \text{ px}^2$, where $\text{px} \equiv \text{pixel size} = 0.06536 \mu\text{m}$). A typical data set has about 14 000–20 000 frames with a total of up to 1 000 000 snapshots of single bacteria. By analyzing those data sets using a parallel cell-tracking algorithm [24], which extracts the full motility history of each tracked bacterium in the field of view, and by analyzing the time dependence of fluorescently labeled Psl trails, we investigate how these trails impact bacterial motility. For better comparability of samples with different numbers of bacteria on the surface, we have measured time in terms of total bacterial visits, i.e., the sum of the number of bacteria in all frames $S_{\text{visits}} = \sum s_i$, where s_i is the number of bacteria present in frame i [24].

The distributions of the two angles $\Delta\theta$ and $\Delta\alpha$ defined in Fig. 1(b) are shown in Figs. 1(c) and 1(d) for 0% and 1% arabinose. Figure 1(d) shows the distributions of the change in bacterial body orientation $\Delta\alpha$ within a 3 s time frame; they appear to be very narrow and mostly independent of the strains in the experiment, which is due to a relatively small rotational diffusion [Fig. S2(b) [37]]. On the other hand, the distribution of the angle between the bacterial trajectory and the body orientation $\Delta\theta$ is wide. Importantly, with increasing Psl deposition the $\Delta\theta$ distribution narrows

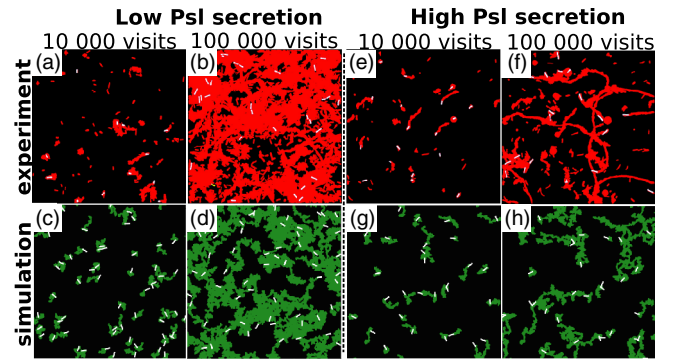


FIG. 2. Snapshots of bacterial positions (white) and surface areas visited over time from experiments (red) and simulations (green) for the case of (a)–(d) low Psl deposition and (e)–(h) high Psl deposition. An enlarged version of this figure can be found in the Supplemental Material [37], Fig. S1. (a),(b) Surface coverage for $\Delta P_{\text{psl}}/P_{\text{BAD-psl}}$ under 0% arabinose. Most of the surface has been visited after a total number of $S_{\text{visits}} = 100\,000$ bacterial visits. (c),(d) Typical simulation outcome for the cases of a low Psl deposition ($k = 0.073 \text{ s}^{-1}$ corresponding to the best fit for 0% arabinose [see Figs. 1(c) and 1(d)]), starting from a random distribution of bacteria. In (d), bacteria explore most of the field. (e),(f) Experimental data for 1% arabinose. The visited area is much smaller, and bacteria tend to aggregate more. (g),(h) A typical simulation outcome of high Psl deposition ($k = 0.18 \text{ s}^{-1}$, corresponding to 1% arabinose), starting from a random distribution. As shown in (h), bacteria aggregate in a small, Psl-rich surface area, making it more attractive for others by secreting more Psl there.

down [see Fig. 1(c)], showing that Psl stabilizes the bacterial trajectory and increases the correlation between orientation of the bacterial body and the moving direction.

We consider a mechanistic model for a rodlike bacterium that pulls itself forward on a surface using pili, taking into account the influence of a bacteria-secreted polysaccharide film on the attachment or detachment of pili, as well as on pulling forces; see the Supplemental Material [37]. The model is an extension of the model in Ref. [33], but here we will specifically focus on *P. aeruginosa* to better understand the experimental results for single-bacterium motion and collective behavior. Each bacterium (labeled a) is assigned a position \mathbf{r}_a and an orientation $\hat{\mathbf{n}}_a = (\cos \varphi_a(t), \sin \varphi_a(t))$ [we can also define a perpendicular unit vector $\hat{\mathbf{n}}_{\perp a} = (-\sin \varphi_a(t), \cos \varphi_a(t))$]. The bacteria secrete Psl trails to which pili can preferentially attach. The attached pili then pull the bacteria forward. The Psl trail has a finite width δ , which we assume to be of the same order as the width of a bacterium. As a result of Psl-dependent attachment or detachment and pulling, pili can propel the bacterium along $\hat{\mathbf{n}}_a$, but also along the Psl gradient $\nabla\psi$, depending on the distribution of pili. In addition, the Psl-dependent pulling will result in an alignment term towards the gradient $\nabla\psi$ [33]. Finally, due to fluctuations in attachment or detachment of bacterial pili, the overall pili pulling force acting on a bacterium will fluctuate; this will introduce noise in the

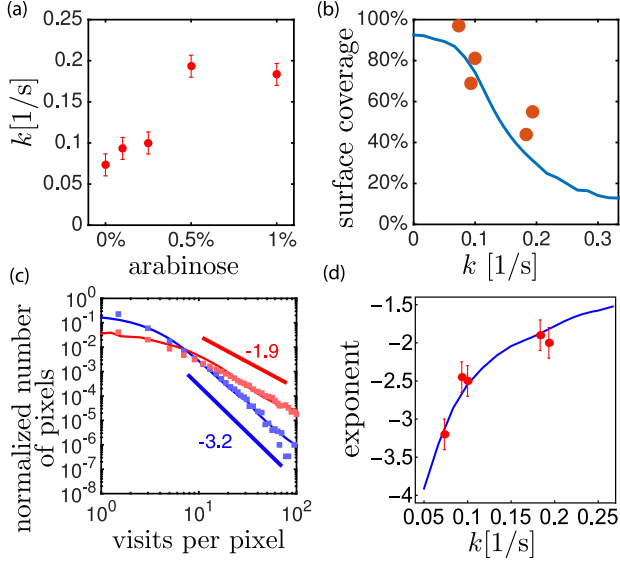


FIG. 3. (a) Experimental arabinose concentrations $C_{\text{ara}} = (0\%, 0.1\%, 0.25\%, 0.5\%, 1\%)$ and the corresponding theoretical values for the Psl secretion $k = (0.073, 0.093, 0.1, 0.19, 0.18) \text{ s}^{-1}$, obtained from the distribution for $\Delta\theta$ and $\Delta\alpha$ at early stages [see Figs. 1(b)–1(d)]. (b)–(d) Comparison between experiments (dots) and theory (lines) for the collective behavior of $\Delta P_{\text{psl}}/P_{\text{BAD-psl}}$. No additional fitting was required to match the experimental results. (b) Surface percentage visited by a colony of 30 bacteria after 13.8 h ($S_{\text{visits}} = 500\,000$ total visits) as a function of Psl deposition rate k . Red dots show experimental data for 0%, 0.1%, 0.25%, 0.5%, and 1% arabinose [for the corresponding k values, see (a)], with an error of $\pm 10\%$ for 0%, 0.1%, and 1% arabinose. For 0.25% and 0.5%, the error could not be determined due to a low sample size. (c) The result of the rich-get-richer mechanism is a power-law distribution in the frequency of visits per pixel, shown for low (blue) and high (red) Psl secretion. Blue: Low Psl secretion at 0% arabinose or $k = 0.073 \text{ s}^{-1}$. Red: High Psl secretion rate at 1% arabinose or $k = 0.18 \text{ s}^{-1}$. The power-law distributions become more hierarchical (slower decay) with increasing Psl. (d) Comparison between experimental (red dots with error bars) and simulated (blue line) power-law exponents. The estimated error of the exponents is ± 0.1 for simulations and ± 0.2 for experiments.

position and orientation Langevin equations, which we approximate as Gaussian. Overall, the equations of motion for the many-body dynamics are constructed as follows [37]:

$$\begin{aligned}
 (d\mathbf{r}_a/dt) &= A(\psi)(\nabla\psi \cdot \hat{\mathbf{n}}_{\perp a})\hat{\mathbf{n}}_{\perp a} + B(\psi)(\nabla\psi \cdot \hat{\mathbf{n}}_a)\hat{\mathbf{n}}_a \\
 &\quad + v(\psi)\hat{\mathbf{n}}_a + \sqrt{2D_{\parallel}(\psi)}\eta_a^{\parallel}\hat{\mathbf{n}}_a + \sqrt{2D_{\perp}(\psi)}\eta_a^{\perp}\hat{\mathbf{n}}_{\perp a}, \\
 (d\hat{\mathbf{n}}_a/dt) &= -\chi(\psi)\hat{\mathbf{n}}_a \times [\hat{\mathbf{n}}_a \times \nabla\psi] + \sqrt{2D_r(\psi)}\eta_a^{\perp}\hat{\mathbf{n}}_{\perp a},
 \end{aligned} \tag{1}$$

and $\partial_t\psi(\mathbf{r}, t) = k\sum_a(1/2\pi\delta^2)e^{-(\mathbf{r}-\mathbf{r}_a)^2/2\delta^2}$. The coefficients are related, and can be written in terms of two independent ones (we choose D_r and v): $\chi = [\gamma_{\parallel}\ell\ell_p(1-c_2)/2\gamma_{\text{rot}}c_1]\partial_{\psi}v$, $D_{\parallel} = [4\gamma_{\text{rot}}^2c_2/(1-c_2)\gamma_{\perp}^2\ell^2]D_r$, $D_{\perp} = (2\gamma_{\text{rot}}/\gamma_{\perp}\ell)^2D_r$,

$A = [\ell_p(1-c_2)\gamma_{\parallel}/c_1\gamma_{\perp}]\partial_{\psi}v$, and $B = [c_2\ell_p/c_1]\partial_{\psi}v$. Here, ℓ is the length of a bacterium, ℓ_p is the length of a pilus, and γ_{\parallel} , γ_{\perp} , γ_{rot} are the friction coefficients for the translation parallel or perpendicular to $\hat{\mathbf{n}}_a$ and for rotational motion. $c_1 = \langle \cos\vartheta \rangle$ and $c_2 = \langle \cos^2\vartheta \rangle$ denote averages involving the distribution of pili angles ϑ relative to the bacterial body axis [see Fig. 1(a)]. The noise terms η_a^{\perp} and η_a^{\parallel} are independent Gaussian white noise of unit strength [37]. We note that the particular geometry for the pili has made the orientational noise identical to the transverse translational noise; see Eq. (1). This is a significant feature of our model. Our choice of a Gaussian shape for the bacterial Psl trail is motivated by the assumption that Psl just secreted from the bacteria will initially diffuse but then the diffusion will come to an effective stop due to stickiness of Psl. Similar models have been applied in previous studies [39].

Experimentally, the length of a bacterium has been determined as $\ell \approx 2 \mu\text{m}$, and the length of a pilus ℓ_p is of the order of the body length. The apparent width of a bacterium has been determined as approximately $0.5 \mu\text{m}$. Since the bacteria are approximately rodlike, we estimate $\gamma_{\perp}/\gamma_{\text{rot}} \approx 5/\ell^2$ [40]. In addition, the anisotropy in friction (perpendicular and parallel to the long axis) is $(\gamma_{\perp} - \gamma_{\parallel})/\gamma_{\parallel} \approx 0.2$ [40] where all values have been rounded. Experimentally, in the absence of EPS secretion we find a diffusion constant $D_{\text{total}0} \approx 1.1 \times 10^{-2} \mu\text{m}^2 \text{ s}^{-1}$ [Fig. S2(a) [37]], which is the result of parallel and perpendicular diffusion $D_{\text{total}0} = D_{\parallel 0} + D_{\perp 0} = D_{\perp 0}[1 + c_2\gamma_{\perp}^2/((1-c_2)\gamma_{\parallel}^2)]$. With $D_r \approx 3.6 \times 10^{-3} \text{ s}^{-1}$ for 0% arabinose [Fig. S2(b) [37]], we get $D_{\perp} \approx 2.3 \times 10^{-3} \mu\text{m}^2 \text{ s}^{-1}$ and $c_2 = \langle \cos^2\vartheta \rangle \approx 0.7$. As an approximation, in our simulations we will set $c_1 = \langle \cos\vartheta \rangle \approx \sqrt{c_2} = 0.8$. The characteristic width of the Gaussian Psl trail has been chosen as $\delta = 0.25 \mu\text{m}$, half the width of the bacterium.

Our microscopic model shows that the dependencies of v and D_r on ψ are controlled by the pili pulling force f , the friction coefficients γ_{\parallel} and γ_{rot} , the attachment rate λ , and the detachment rate μ : $v(\psi) \propto f\lambda/[\gamma_{\parallel}(\lambda + \mu)]$ and $D_r(\psi) \propto f^2\lambda\mu/[\gamma_{\text{rot}}^2(\lambda + \mu)^3]$ (see the Supplemental Material [37]). While, in principle, all of these quantities depend on ψ , we can make some intuitive assumptions about the general trends; e.g., the friction coefficients increase with ψ , and better attachment to Psl implies the attachment rate increases and the detachment rate decreases as ψ is increased. This, in turn, suggests that by extracting information about the dependence of v and D_r on ψ from experiments, we can gather information about the above mentioned components. If the Psl concentrations are small, we can Taylor approximate $v \approx v_0 + v_1\psi$ and $D_r \approx D_{r0} + D_{r1}\psi$. For a mutant without any EPS secretion, the experimental data for the translational mean square displacement show no propulsive component of the motion at the shortest time scale that we have resolved [Fig. S2(a) [37]], and hence we conclude that in the absence of Psl, the velocity component $v_0 \approx 0$.

We therefore model the velocity as $v = v_1\psi$. This also implies that $A(\psi)$, $B(\psi)$, and $\chi(\psi)$ are larger than 0 for nonzero EPS secretion. In addition, noting that the rotational diffusion D_r varies only weakly between 0% and 1% arabinose, we set $D_{r1} \approx 0$, which also introduces nonzero translational diffusion constants D_{\parallel} and D_{\perp} .

We performed Brownian dynamics simulations of the dynamical equations with the above choices for the coefficients and parameters. Note that the Psl deposition strength k always appears in combination with v_1 and hence does not constitute an additional parameter. This leaves us with the one parameter kv_1 to be determined. In our simulations, we only varied the Psl deposition k and set $v_1 = 1 \text{ px}^3/\text{frame} = 9.3 \times 10^{-5} \mu\text{m}^3 \text{ s}^{-1}$. The parameters in the numerical simulations were chosen such that they correspond to the experimental parameters. The unit of length was $1 \text{ px} = 0.06536 \mu\text{m}$, and the unit of time was $1 \text{ frame} = 3 \text{ s}$. For all our simulations, we regarded the above parameters as characteristic constants of the bacteria and only varied k between simulation runs to emulate a situation where the amount of Psl produced depends on an external factor (like the arabinose concentration on the substrate for the $\Delta P_{psl}/P_{\text{BAD-}psl}$ mutant).

Figures 1(c) and 1(d) show the angle distributions for $\Delta\theta$ and $\Delta\alpha$ from experiments and simulations. The qualitative characteristics from the experiments, in particular, the very narrow distribution for $\Delta\alpha$, the wide distribution for $\Delta\theta$, and the narrowing down of $\Delta\theta$ with increasing Psl deposition, have been reproduced. As highlighted in the Supplemental Material [37], the translational and alignment terms proportional to $\nabla\psi$ in Eq. (1) confine the bacteria to the trail center and enable them to follow trails of other bacteria, thus increasing the correlation between the trail and body orientation at long times. Comparison between simulations and experiments suggests that the experimental data for low Psl deposition (0% arabinose) best correspond to $k = 0.073 \text{ s}^{-1}$ [Fig. 1(c)], whereas the data for high Psl deposition (1% arabinose concentration) are best matched by $k = 0.18 \text{ s}^{-1}$ [Fig. 1(d)]. The corresponding k values for other arabinose concentrations are shown in Fig. 3(a).

On a larger scale, studies using single-particle tracking have shown that the type IV pili-mediated twitching motility of *P. aeruginosa* plays an essential role in the early stages of biofilm formation due to complex interactions with secreted Psl. The result of this is a “rich-get-richer mechanism” which helps *P. aeruginosa* accumulate at just a few sites, whereas other sites are not visited at all or visited infrequently. To put our microscopic model to a stringent test, we compare the long-time prediction of the simulation with the corresponding results from our experiments without any additional fitting or adjustments. We find that the simulations predict exactly the same behavior as we observe experimentally, including the power-law distribution of visited sites and the percentage of surface coverage; see Figs. 3(b)–3(d). Figures 2(a)–2(h)

show a typical Psl field $\psi(\mathbf{r}, t)$ over a long period of time. In Figs. 2(a)–2(d), the Psl deposition strength is very small, which makes the bacterial behavior essentially diffusive for long times. Therefore, in the long run, the spatial distribution of Psl is relatively uniform since the bacteria are not attracted to any particular sites. This is reflected in a high surface coverage over time [Fig. 3(b)], as well as a relatively small power-law exponent for the distribution [Figs. 3(c) and 3(d)].

On the other hand, in Figs. 2(e)–2(h), which show the Psl field ψ for a large Psl deposition rate, sites are preferentially visited where bacteria have already been previously, due to the strong interaction with the Psl field. As a result, bacteria visit a smaller fraction of sites [Fig. 3(b)]. Analyzing the distribution of total bacterial visits to a given pixel, one observes a power-law behavior when plotting the total visits per pixel against the number of pixels with this visit frequency. For an increasing Psl deposition rate, the exponent increases, which implies a less egalitarian visit distribution, i.e., many sites with very few bacterial visits and a few sites where bacteria aggregate and spend a long period of time. This leads to a hierarchical Psl distribution, with a larger power-law exponent [Figs. 3(c) and 3(d)]. The distribution of visits is directly related to the distribution of Psl concentrations per pixel [24].

The distribution of bacterial visits to surface sites (and consequently the Psl concentration) has the hallmarks of a Pareto-type power-law distribution, similar to wealth distributions in capitalist economies [24,41]. Moreover, experiments with the $\Delta P_{psl}/P_{\text{BAD-}psl}$ mutant, which produces Psl depending on the arabinose concentration on the substrate (varied between 0% and 1%), suggest that the corresponding power-law exponents change from -3.1 to -1.8 , making the Psl and surface visit distributions more hierarchical with increasing Psl deposition [24]. Theoretical and experimental exponents are in good quantitative agreement, as seen in Fig. 3(d). The simulations for Figs. 3(b)–3(d) were performed on a field with 30 bacteria for 16667 frames; i.e., a total of $S_{\text{visits}} = 500\,000$.

In summary, based on microscopic interactions observed in *P. aeruginosa* experiments, we have shown that the microcolony formation can be a direct consequence of trail deposition and pili-mediated motility, without any active signal processing by the bacteria. This leads to efficient surface exploration and self-organization. We have found that the combination of translational and orientational gradient response facilitates social trail following and thus quantitatively explains crucial effects at the early stages of microcolony formation. We expect these trail-induced motility effects to strongly modify the complex motility from competitive deployment of multiple type IV pili [42]. Our results have a broad range of impact, ranging from self-guided active matter to bacterial biofilm microbiology to embryonic development.

This work was supported by the Human Frontier Science Program RGP0061/2013, the Ernst Ludwig Ehrlich Studienwerk (A. G.), the Tianjin Municipal Natural Science Foundation Grant No. 15JCZDJC41100 (K. Z.), and the Office of Naval Research Grant No. N000141410051 (G. C. L. W.). We acknowledge the COST Action MP1305 “Flowing Matter.”

*gclwong@seas.ucla.edu

†ramin.golestanian@physics.ox.ac.uk

- [1] D. Woodward, R. Tyson, M. Myerscough, J. Murray, E. Budrene, and H. Berg, *Biophys. J.* **68**, 2181 (1995).
- [2] M. P. Brenner, L. S. Levitov, and E. O. Budrene, *Biophys. J.* **74**, 1677 (1998).
- [3] E. Ben-Jacob, I. Cohen, and H. Levine, *Adv. Phys.* **49**, 395 (2000).
- [4] C. Liu, X. Fu, L. Liu, X. Ren, C. K. Chau, S. Li, L. Xiang, H. Zeng, G. Chen, L.-H. Tang *et al.*, *Science* **334**, 238 (2011).
- [5] Y. Zhang, A. Ducret, J. Shaevitz, and T. Mignot, *FEMS Microbiol. Rev.* **36**, 149 (2012).
- [6] J. Taktikos, V. Zaburdaev, and H. Stark, *Phys. Rev. E* **85**, 051901 (2012).
- [7] M. Vergassola, E. Villermaux, and B. I. Shraiman, *Nature (London)* **445**, 406 (2007).
- [8] A. Gelimson and R. Golestanian, *Phys. Rev. Lett.* **114**, 028101 (2015).
- [9] R. Golestanian, *Phys. Rev. Lett.* **108**, 038303 (2012).
- [10] J. A. Cohen and R. Golestanian, *Phys. Rev. Lett.* **112**, 068302 (2014).
- [11] S. Saha, R. Golestanian, and S. Ramaswamy, *Phys. Rev. E* **89**, 062316 (2014).
- [12] O. Pohl and H. Stark, *Phys. Rev. Lett.* **112**, 238303 (2014).
- [13] V. Sourjik and H. C. Berg, *Nature (London)* **428**, 437 (2004).
- [14] H. Levine and W.-J. Rappel, *Phys. Today* **66**, No. 2, 24 (2013).
- [15] L. Ma, K. D. Jackson, R. M. Landry, M. R. Parsek, and D. J. Wozniak, *J. Bacteriol.* **188**, 8213 (2006).
- [16] L. Ma, H. Lu, A. Sprinkle, M. R. Parsek, and D. J. Wozniak, *J. Bacteriol.* **189**, 8353 (2007).
- [17] M. S. Byrd, I. Sadovskaya, E. Vinogradov, H. Lu, A. B. Sprinkle, S. H. Richardson, L. Ma, B. Ralston, M. R. Parsek, E. M. Anderson *et al.*, *Mol. Microbiol.* **73**, 622 (2009).
- [18] L. L. Burrows, *Annu. Rev. Microbiol.* **66**, 493 (2012).
- [19] B. Maier and G. C. Wong, *Trends Microbiol.* **23**, 775 (2015).
- [20] G. A. O’Toole and R. Kolter, *Mol. Microbiol.* **30**, 295 (1998).
- [21] J. M. Skerker and H. C. Berg, *Proc. Natl. Acad. Sci. U.S.A.* **98**, 6901 (2001).
- [22] F. Jin, J. C. Conrad, M. L. Gibiansky, and G. C. Wong, *Proc. Natl. Acad. Sci. U.S.A.* **108**, 12617 (2011).
- [23] M. L. Gibiansky, W. Hu, K. A. Dahmen, W. Shi, and G. C. Wong, *Proc. Natl. Acad. Sci. U.S.A.* **110**, 2330 (2013).
- [24] K. Zhao, B. S. Tseng, B. Beckerman, F. Jin, M. L. Gibiansky, J. J. Harrison, E. Luijten, M. R. Parsek, and G. C. Wong, *Nature (London)* **497**, 388 (2013).
- [25] M. E. Cates and J. Tailleur, *Annu. Rev. Condens. Matter Phys.* **6**, 219 (2015).
- [26] H. Chaté, F. Ginelli, G. Grégoire, and F. Raynaud, *Phys. Rev. E* **77**, 046113 (2008).
- [27] H. P. Zhang, A. Beér, E.-L. Florin, and H. L. Swinney, *Proc. Natl. Acad. Sci. U.S.A.* **107**, 13626 (2010).
- [28] F. Peruani, J. Starruss, V. Jakovljevic, L. Sogaard-Andersen, A. Deutsch, and M. Bär, *Phys. Rev. Lett.* **108**, 098102 (2012).
- [29] J. Starruss, F. Peruani, V. Jakovljevic, L. Sogaard-Andersen, A. Deutsch, and M. Bär, *Interface Focus* **2**, 774 (2012).
- [30] S. Thutupalli, M. Sun, F. Bunyak, K. Palaniappan, and J. W. Shaevitz, *Royal Soc. Interface* **12**, 0049 (2015).
- [31] P. Ghosh, J. Mondal, E. Ben-Jacob, and H. Levine, *Proc. Natl. Acad. Sci. U.S.A.* **112**, E2166 (2015).
- [32] M. Marchetti, J. Joanny, S. Ramaswamy, T. Liverpool, J. Prost, M. Rao, and R. A. Simha, *Rev. Mod. Phys.* **85**, 1143 (2013).
- [33] W. T. Kranz, A. Gelimson, K. Zhao, G. C. L. Wong, and R. Golestanian, *Phys. Rev. Lett.* **117**, 038101 (2016).
- [34] B. Holloway, *J. Gen. Microbiol.* **13**, 572 (1955).
- [35] A. Heydorn, B. K. Ersbøll, M. Hentzer, M. R. Parsek, M. Givskov, and S. Molin, *Microbiol.* **146**, 2409 (2000).
- [36] S. A. Cruz, R. Popat, M. T. Rybtke, M. Cámara, M. Givskov, T. Tolker-Nielsen, S. P. Diggle, and P. Williams, *Biofouling* **28**, 835 (2012).
- [37] See Supplemental Material at <http://link.aps.org/supplemental/10.1103/PhysRevLett.117.178102>, which includes Ref. [38], for the details of our microscopic model and the derivation of the mesoscopic equations of motion.
- [38] N. Van Kampen, *J. Stat. Phys.* **24**, 175 (1981).
- [39] I. Couzin and N. Franks, *Proc. R. Soc. B Bio.* **270**, 139 (2003).
- [40] M. M. Tirado, C. López Martínez, and J. García de la Torre, *J. Chem. Phys.* **81**, 2047 (1984).
- [41] M. E. Newman, *Contemp. Phys.* **46**, 323 (2005).
- [42] C. Holz, D. Opitz, L. Greune, R. Kurre, M. Koomey, M. A. Schmidt, and B. Maier, *Phys. Rev. Lett.* **104**, 178104 (2010).